The Astrophysical Journal Supplement Series, 238:18 (10pp), 2018 October https://doi.org/10.3847/1538-4365/aadcae
© 2018. The American Astronomical Society. All rights reserved.

The Carrier of 3.3 μm Aromatic Infrared Bands: Anharmonicity and Temperature Effects on Neutral PAHs

Tao Chen[1,2]
[1] Leiden University, Leiden Observatory, Niels Bohrweg 2, NL-2333 CA Leiden, The Netherlands; chen@strw.leidenuniv.nl
[2] School of Engineering Sciences in Chemistry, Biotechnology and Health, Department of Theoretical Chemistry & Biology, Royal Institute of Technology, SE-10691, Stockholm, Sweden
Received 2018 July 19; revised 2018 August 19; accepted 2018 August 21; published 2018 October 1

Abstract

Anharmonic infrared (IR) spectra are crucial for the study of interstellar polycyclic aromatic hydrocarbon (PAH) molecules. This work aims to provide a comprehensive study of the features that may influence the accuracy of anharmonic IR spectra of PAHs so that a reliable spectrum that incorporates all necessary features for interpreting the observational IR spectra can be obtained. Six PAHs are investigated: naphthalene, anthracene, pyrene, chrysene, 9,10-dimethylanthracene, and 9,10-dihydroanthracene. The NIST spectra and high-resolution IR absorption spectra are utilized as the reference for the comparisons. The influences of different resonances and resonant thresholds are studied. Four methods for electronic structure calculations are tested. The quantitative comparisons indicate that for the NIST data, B3LYP/N07D provides the best agreement with measured spectra concerning band positions and B3LYP/cc-pVTZ is superior in the description of the relative intensities. The importance of 1–3 Darling–Dennison resonances, which are required for generating triple combination bands, is investigated through a comparison to a high-resolution experimental spectrum. For interpreting the bandwidths and profiles of the observational spectra, the temperature effects are included through the Wand-Landau random walk technique. The comparisons between calculated high-temperature anharmonic and observational spectra indicate that small and compact PAHs might be responsible for the 3.3 μm aromatic infrared bands.

Key words: astrochemistry – infrared: ISM – ISM: molecules – line: identification – line: profiles – techniques: spectroscopic

1. Introduction

Polycyclic aromatic hydrocarbon (PAH) molecules are a family of molecules consisting of more than two fused benzenoid rings with hydrogen atoms attached around the free edges. They are of high interest in several fields of research, e.g., combustion chemistry (Richter & Howard 2000), environmental science (Srogi 2007), solar cell technology (Wang et al. 2008), and molecular electronics (Kubatkin et al. 2003). In space, many observations suggest that PAHs are present in comets (Li 2009), and in the interstellar medium (ISM) as the carriers of the strong infrared emission features from galactic and extragalactic objects (Allamandola et al. 1989; Tielens 2008; Boersma et al. 2013). As our knowledge of interstellar PAHs comes mainly from IR observations, much effort has been devoted over the last three decades to determining the IR spectra of PAHs and their dependence on molecular characteristics (Tielens 2013).

The standard approach, in the framework of Density Functional Theory (DFT), that is used to compute IR spectra, consists of quantum chemical calculations in the static double harmonic approximation as implemented in most major computational chemistry packages. However, in this approach, the anharmonic effects on the fundamental modes are not taken into account, and band combinations and overtones are disregarded. One or more scaling factors are often applied to the computed harmonic frequencies to reduce the difference with experimental values (Langhoff 1996). As a first-order approximation, this approach could reproduce the overall low-resolution IR spectrum of individual PAHs, but serious problems appear when a comparison is made with high-resolution experiments (Mackie et al. 2016).

Several methods have been proposed to include explicitly anharmonic effects in quantum chemistry vibrational frequency calculations, e.g., the vibrational self-consistent field (Bowman 1978), followed by a second-order perturbation-corrected theory (Jung & Gerber 1996; Yagi et al. 2000) for weak coupling between modes or by a vibrational configuration interaction (Christoffel & Bowman 1982) in the case of very strong coupling. Vibrational second-order perturbation theory (VPT2) utilizes quadratic, all relevant cubic, and quartic force constants to create a quartic force field from which anharmonic vibrational frequencies of polyatomic molecules can be calculated. Due to the high computational cost, VPT2 is commonly used for the study of the medium and large-size molecules (Barone et al. 2014; Mackie et al. 2015, 2016). Based on VPT2, several versions are developed: e.g., C-VPT2 (Krasnoshchekov et al. 2014), VPT2+K (Rosnik & Polik 2014), DCPT2 (Assfeld et al. 1995), etc. (Clabo et al. 1988; Allen et al. 1990; Amos et al. 1991; Gaw et al. 1996; Barone 2005; Barone et al. 2010). In addition, a generalized vibrational second-order perturbation theory (GVPT2) is developed, in which the near-resonant terms are removed, and the removed terms are treated variationally (Barone 2005; Barone et al. 2010; Bloino & Barone 2012; Bloino et al. 2012).

Recent work has shown that VPT2 is a reliable method for producing anharmonic IR spectra of semi-rigid, and isolated systems, especially for low-lying vibrational states (i.e., fundamental bands, overtones and combination bands; Lee et al. 1995; Martin et al. 1998; Barone et al. 2014). Comparison of the calculated VPT2 results with their experimental counterparts suggests that remarkably accurate anharmonic contributions can be obtained with certain functionals and basis sets for small and medium-sized molecules (Barone et al. 2014; Mackie et al. 2015; Ravichandran & Banik 2018). However, the application of VPT2 to PAHs shows appreciable discrepancy in comparison to

experimental spectra, which could be due to the improper choice of functionals and basis sets. It has been reported that for hydrogenated and methylated PAHs, changing from B971/TZ2P to B3LYP/N07D, the improvement in agreement between theory and experiment was found to be from an error of 1% down to 0.1% (30–3 cm^{-1} in the CH-stretching region; Mackie et al. 2018).

The resonances and order-of-combination bands play a vital role in interpreting the high-resolution experimental IR spectra. Recent work shows that the calculated anharmonic spectra with double combination bands underpredict the number of bands and their relative intensities and it has been suggested that this is the result of neglecting triple combination bands (Maltseva et al. 2015).

In addition to anharmonicity and resonances, temperature effects are indispensable for understanding the aromatic infrared bands (AIBs), as the PAHs are believed to be highly excited in the ISM through absorption of visible/UV photons (Tielens 2008). To incorporate temperature effects into the IR spectra, the Wang-Landau method is used to handle high-dimensional space problems (Wang & Landau 2001). It has been shown that this method reproduces accurate vibrational state densities for large, nonseparable systems (Basire et al. 2009). However, only fundamental bands were considered in previous studies, and the resonances and combination bands are missing.

To provide and validate a computational strategy for PAH molecules, in this work, we study the influences of functionals, basis sets, resonant thresholds, order-of-combination bands, and temperature effects on the IR spectra of PAHs. Considering all of these factors, the observational AIBs should be unambiguously interpreted.

2. Computational Details

The calculations included in this work are based on DFT as implemented in the Gaussian 16 package (Frisch et al. 2016). We choose the functionals of B3LYP (Lee et al. 1988; Becke 1992) and B971 (Hamprecht et al. 1998) for this work, as they are commonly used for study of PAHs (Bauschlicher et al. 2008; Ricca et al. 2012; Mackie et al. 2015). The basis sets of N07D (Barone & Cimino 2008), cc-pVTZ (Dunning 1989), and TZ2P (Dunning 1971) are utilized for the comparisons. The N07D basis set is a polarized double-ζ basis set that has been introduced with the aim of enabling cost-effective computation of spectroscopic properties for medium-to-large molecular systems (Barone et al. 2014). The B971 functional in conjunction with the TZ2P basis set has recently been validated through comparison with high-resolution, low-temperature gas-phase experimental spectra (Mackie et al. 2015, 2016). The basis set of cc-pVTZ provides an accurate description of the rotational energy levels in the ground and low-energy excited vibrational states of PAHs and their N-substituted derivatives (Gruet et al. 2015). The dispersion-corrected B3LYP-D3 (Grimme et al. 2011) is considered in this work as well. This correction is commonly used for the study of weakly bonded systems. It is of great interest to investigate how such weak interaction affect the subtle vibrations, especially the effects on anharmonic IR spectra.

Vibrational anharmonicities, mode couplings, and resonances can significantly affect the spectra, especially for those systems with many vibrational resonances, such as PAH molecules. To account for these effects, the first three non-zero terms of the Taylor expansion of vibrational potential energy surface need to be considered (Csaszar 2012):

$$\begin{aligned} V = & \sum_{i=1}^{3N}\left(\frac{\partial V}{\partial q_i}\right)_{V_0} q_i - \frac{1}{2}\sum_{i=1}^{3N}\sum_{j=1}^{i}\left(\frac{\partial^2 V}{\partial q_i \partial q_j}\right)_{V_0} q_i q_j \\ & + \frac{1}{6}\sum_{i=1}^{3N}\sum_{j=1}^{i}\sum_{k=1}^{j}\left(\frac{\partial^3 V}{\partial q_i \partial q_j \partial q_k}\right)_{V_0} q_i q_j q_k \\ & + \frac{1}{24}\sum_{i=1}^{3N}\sum_{j=1}^{i}\sum_{k=1}^{j}\sum_{l=1}^{k}\left(\frac{\partial^3 V}{\partial q_i \partial q_j \partial q_k \partial q_l}\right)_{V_0} q_i q_j q_k q_l. \end{aligned} \quad (1)$$

Typically, this expansion is done at the geometrical minimum, so that the gradient, i.e., the first term in Equation (1), is zero. The third and fourth derivatives of the potential energy V with respect to the dimensionless normal coordinates Q, are also referred to as cubic and quartic force constants:

$$k_{ijk} = \frac{\partial^3 V}{\partial q_i \partial q_j \partial q_k},\ k_{ijkl} = \frac{\partial^4 V}{\partial q_i \partial q_j \partial q_k \partial q_l}. \quad (2)$$

For an asymmetric top, the diagonal terms of the anharmonic χ matrix can be found with the following formula (Amos et al. 1991; Maslen et al. 1992; Barone 2004; Bloino et al. 2012):

$$16\chi_{ii} = k_{iiii} - \frac{5k_{iii}^2}{3\omega_i} - \sum_{j\neq i}^{N}\frac{(8\omega_i^2 - 3\omega_j^2)k_{iij}^2}{\omega_j(4\omega_i^2 - \omega_j^2)}. \quad (3)$$

And the off-diagonal terms are:

$$\begin{aligned} 4\chi_{ij} = & k_{iijj} - \frac{2\omega_i k_{iij}^2}{4\omega_i^2 - \omega_j^2} - \frac{2\omega_j k_{ijj}^2}{4\omega_j^2 - \omega_i^2} - \frac{k_{iii}k_{ijj}}{\omega_i} - \frac{k_{jjj}k_{iij}}{\omega_j} \\ & + \sum_{k\neq i,j}^{N}\left[\frac{2\omega_k(\omega_i^2 + \omega_j^2 - \omega_k^2)k_{ijk}^2}{\Delta_{ijk}} - \frac{k_{iik}k_{jjk}}{\omega_k}\right] \\ & + \frac{4(\omega_i^2 + \omega_j^2)}{\omega_i\omega_j}\sum_{\tau=x,y,z} B_e^{\tau}(\zeta_{ij}^{\tau})^2, \end{aligned} \quad (4)$$

where

$$\Delta_{ijk} = \omega_i^4 + \omega_j^4 + \omega_k^4 - 2(\omega_i^2\omega_j^2 + \omega_i^2\omega_k^2 + \omega_j^2\omega_k^2) \quad (5)$$

ω_i is the harmonic wavenumber (in cm^{-1}) associated with mode i, B_e^{τ} is the diagonal inertial tensor of the molecule at equilibrium geometry, and ζ_{ij}^{τ} is the Coriolis constant coupling modes i and j along the rotation axis I_t.

Knowing these parameters, for a system with N internal degrees of freedom, the vibrational energies of the states of interest can be found as follows (Amos et al. 1991; Barone 2005). Fundamental:

$$\nu_{1_i} = \omega_i + 2\chi_{ii} + \frac{1}{2}\sum_{j\neq i}^{N}\chi_{ij}. \quad (6)$$

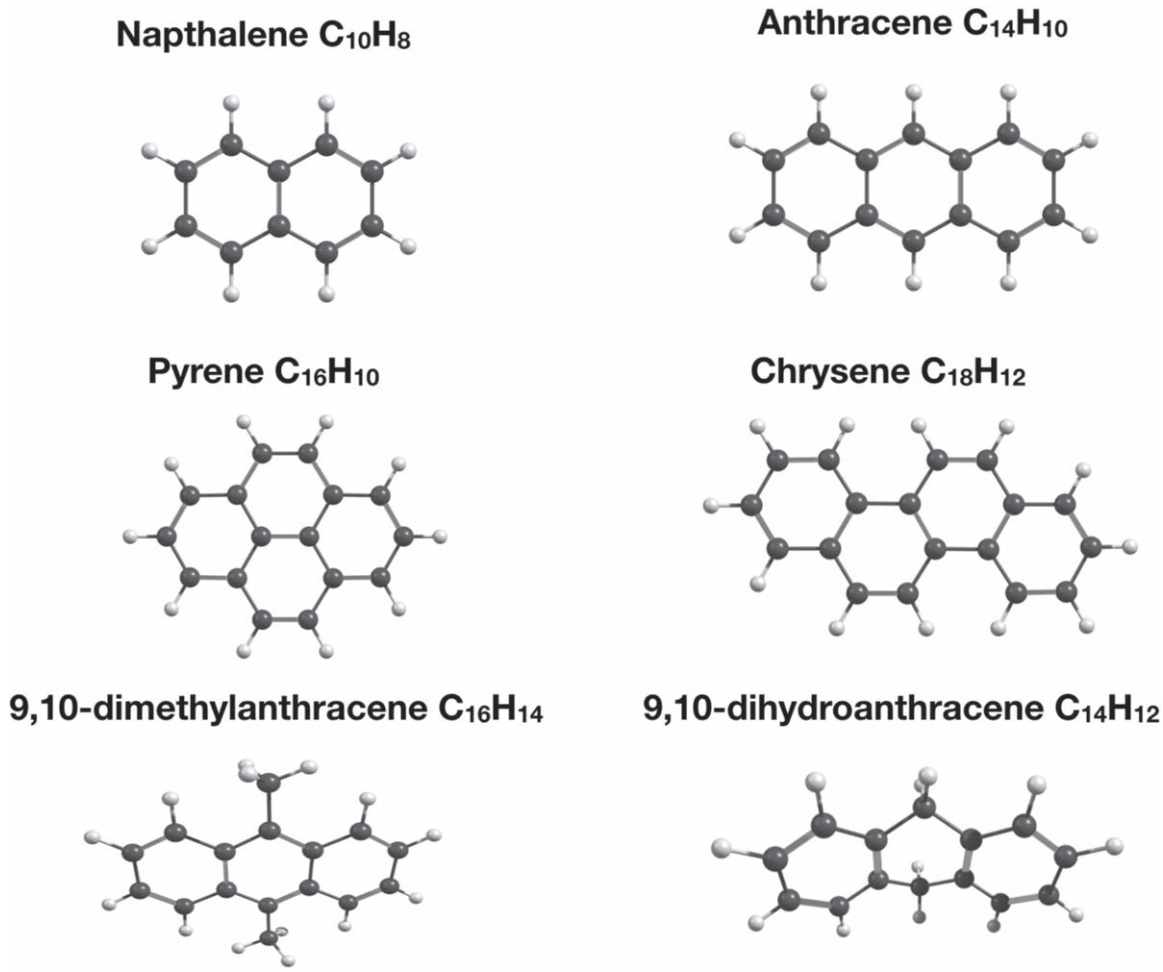

Figure 1. The molecules studied in this work. Naphthalene and anthracene are linear molecules. Pyrene and chrysene are nonlinear molecules. 9,10-dimethylanthracene and 9,10-dihydroanthracene are functionalized/decorated molecules.

Overtones:

$$\nu_{2_i} = 2\omega_i + 6\chi_{ii} + \sum_{j\neq i}^{N} \chi_{ij}. \quad (7)$$

Combination bands:

$$\nu_{1_i 1_j} = \omega_i + \omega_j + 2\chi_{ii} + 2\chi_{jj} + 2\chi_{ij} + \frac{1}{2}\sum_{k\neq i,j}^{N} [\chi_{ik} + \chi_{jk}] = \nu_{1_i} + \nu_{1_j} + \chi_{ij}. \quad (8)$$

The geometry optimizations are performed with a very tight convergence criterion and fine-grid (Int = 200,974) numerical integrations. For the resonant calculation, the generalized VPT2 (GVPT2) approach (Barone et al. 2014) is adopted for this work. GVPT2 involves a two-step procedure: first, resonant terms are identified by means of an ad hoc test (Martin et al. 1995) and successively removed, which is called deperturbed VPT2 (DVPT2). In the second step, the discarded terms are reintroduced through a variational treatment. This approach has been recognized to give very accurate results (Maslen et al. 1992; Martin et al. 1995; Boese & Martin 2004; Barone et al. 2014; Mackie et al. 2015, 2016).

3. Results and Discussion

Figure 1 shows the structures of the studied molecules in this work. These molecules are selected, as they are representative of three PAH subgroups: naphthalene and anthracene represent the smallest linear PAHs; pyrene is the smallest compact molecule and together with chrysene, they are nonlinear PAHs; 9,10-dimethylanthracene and 9,10-dihydroanthracene are functionalized/decorated PAHs.

3.1. Resonant Thresholds

Four types of resonances are considered in this work. First, there are 1–2 Fermi resonances, which occur when the wavenumber of a mode is nearly equal to the sum of the wavenumbers of two modes ($\omega_i \approx \omega_j + \omega_k$). Second, there are 1–1 Darling–Dennison resonances, which occur when the wavenumber of a mode is equal to the wavenumbers of another one ($\omega_i \approx \omega_j$); these are are responsible for double combination bands. Next, there 1–3 Darling–Dennison resonances, which occur when the wavenumber of a mode is approximately equal to the sum of the wavenumbers of three modes ($\omega_i \approx \omega_j + \omega_k + \omega_l$). Finally, there are 2–2 Darling–Dennison resonances, which occur when the sum of the wavenumbers of two modes is equal to the sum of the wavenumbers of another two modes ($\omega_i + \omega_j \approx \omega_k + \omega_l$); these are responsible for triple combination bands. The maximum and minimum frequency thresholds for these

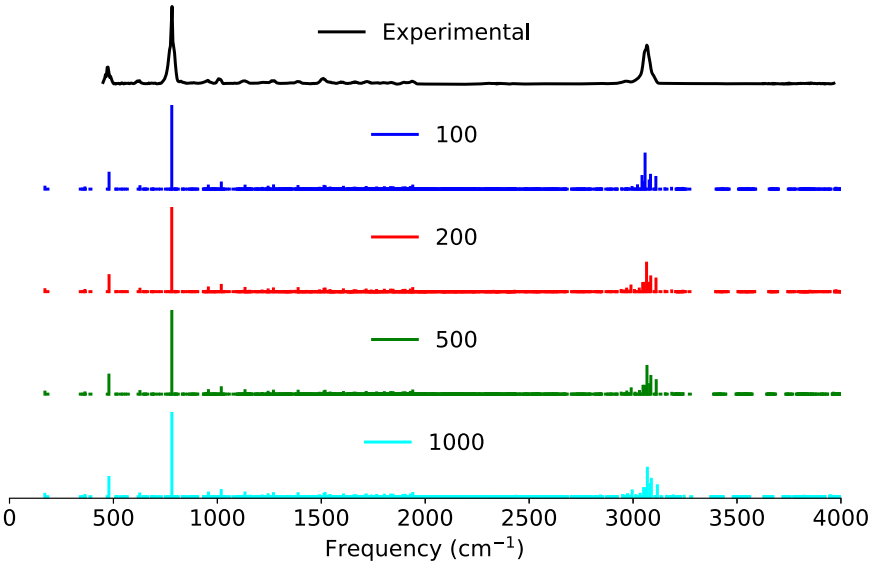

Figure 2. Calculated anharmonic spectra (B3LYP/N07D) of naphthalene with different resonance thresholds in comparison to NIST experimental data.

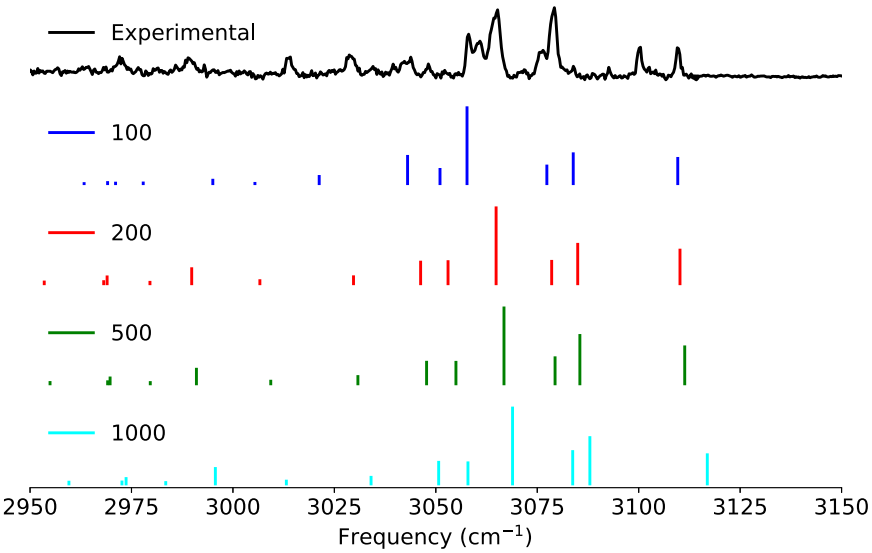

Figure 3. Calculated anharmonic spectra (B3LYP/N07D) of naphthalene with different resonance thresholds in comparison to high-resolution experimental data.

resonances can be adjusted to achieve the best agreement with the high-resolution experimental spectra (Maltseva et al. 2015, 2016). Figure 2 shows the calculated anharmonic spectra with double combination bands of naphthalene in comparison with experimental spectra downloaded from the NIST Chemistry WebBook (Linstrom & Mallard 2001). Four maximum resonant threshold values are tested: 100, 200, 500, and 1000 cm^{-1}. The minimum frequency thresholds are set to 0 cm^{-1}. The general profiles of the spectra do not change with increasing of the thresholds, and all of them agree well with the experimental spectra.

Figure 3 shows the zoomed-in region of 2900–3200 cm^{-1}, which is the C–H stretching region dominated by anharmonicity and resonances. A clear trend can be seen when the resonance thresholds increase, especially for the highest peak in this region, which shifts to the right side of the spectrum, e.g., the highest peak shifts from 3057.7 cm^{-1} to 3064.9 cm^{-1}, 3066.8, and 3068.9 cm^{-1}, correspondingly. We choose the threshold value of 200 cm^{-1} for the following study, as it presents reasonable band positions and relative intensities, and it takes reasonable computational time and memory. A higher threshold incorporates more interactions, which leads to a larger interaction matrix to calculate, possibly causing greater consumption of computational time and memory. Also, the computational time and memory increase significantly with the size of the molecule.

3.2. Functionals and Basis Sets

To investigate the influence of different methods, the NIST data are utilized as a reference for the comparisons (Linstrom & Mallard 2001). Moreover, each of the molecules shown in Figure 1 has also been measured at high-resolution spectra in the C–H stretching region (Maltseva et al. 2015, 2016) and this region is particularly sensitive to resonances and anharmonic effects (Mackie et al. 2015, 2016).

Figure 4 shows the histogram collecting the percentual band shift between experiments and theory for the molecules in Figure 1 with different functional/basis sets. The NIST data are utilized as a reference (Linstrom & Mallard 2001). Each

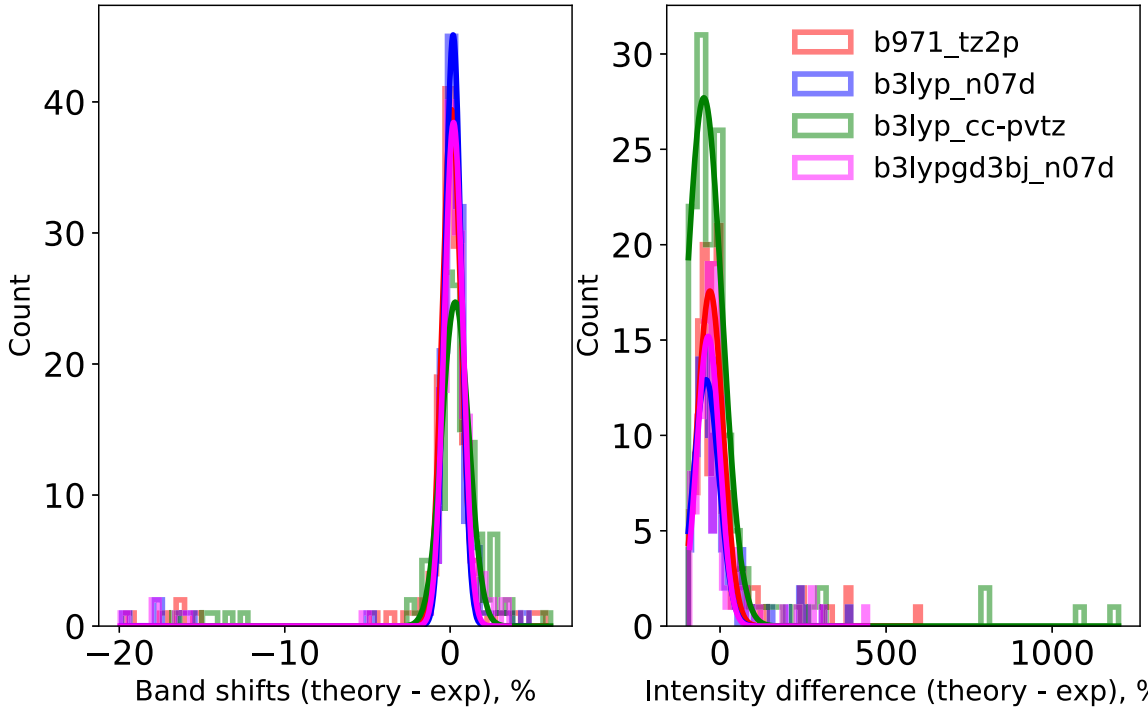

Figure 4. Histogram showing the differences between the line positions and intensities of the anharmonic theory (with different functionals and basis sets) and the NIST gas-phase experiments. For quantitative comparison of the histograms, Gaussian fittings are added for each histogram.

histogram is fit by a Gaussian function. All the tested methods have a reasonable agreement with the experimental data concerning the peak positions. B3LYP/N07D has the highest and thinnest Gaussian profile, with a height of ∼45, μ of 0.18, and center 0.49%. B971/TZ2P comes next, with a height of ∼39, μ of 0.09, and center 0.57%. The third one regarding Gaussian height is B3LYP-D3/N07D. The worst one is B3LYP/cc-PVTZ. The right panel of Figure 4 shows the histograms for the intensity differences between calculated and experimental spectra. B3LYP/cc-PVTZ shows the best agreement with the intensities of experimental spectra. The second best method is B3LYP/N07D. Then come B3LYP-D3/N07D and B971/TZ2P. See Table 1 for more information about the Gaussian fitting parameters of the functionals and basis sets. Large discrepancies (>500%) between theory and experiments are observed mainly between the differences at the C–H stretching region; see the spectra comparisons in previous works for details (Mackie et al. 2015, 2016, 2018).

It has been observed recently that due to the inclusion of methyl rotors the methylated PAHs behave differently from a regular PAH (Mackie et al. 2018). Therefore, the decorated PAHs and regular PAHs are studied separately. Figure 5 compares the band position shifts and relative intensity changes for regular PAHs. As shown in Figure 3, due to the limitations of experimental techniques, high-resolution spectra are only available for a short wavenumber range, 2900–3200 cm^{-1} for regular PAHs, and 2750–3200 cm^{-1} for decorated PAHs (Maltseva et al. 2015, 2016); only a few clear bands can be identified in the high-resolution spectra, which lead to poor statistics for the histograms. We only manage to fit the histogram for position shifts. It is clear that B3LYP/cc-PVTZ is superior to any other tested methods. See Table 2 for more information about the Gaussian fitting parameters of the functionals and basis sets. For the relative intensities, due to the shortage of data points and wide distribution of the histogram, no successful Gaussian fitting is found. However, it is clear that B971/TZ2P shows the highest bar on the histogram.

Table 1
Parameters of Gaussian Profiles for Histograms Associated with NIST Data

	Positions $Ae^{\frac{-(x-\mu)^2}{2\sigma^2}}$			Intensities $Ae^{\frac{-(x-\mu)^2}{2\sigma^2}}$		
Methods	A	μ	σ	A	μ	σ
B971/TZ2P	39.41	0.09	0.57	17.57	−30.43	38.65
B3LYP/N07D	45.11	0.18	0.49	12.92	−42.11	38.83
B3LYP/cc-PVTZ	24.72	0.31	0.81	27.70	−48.66	54.84
B3LYP-D3/N07D	38.43	0.20	0.56	15.19	−35.74	34.56

Figure 6 shows the histogram for 9,10-dimethylanthracene and 9,10-dihydroanthracene. Again, due to the poor statistics, no successful Gaussian fitting is achieved. However, judging by the distribution of the data, B3LYP-D3/N07D is the most accurate method for the description of the band positions, and B3LYP/cc-PVTZ is the most accurate method for the description of the relative intensities.

3.3. Combination Bands

It has been observed that the calculated anharmonic spectra with double combination bands underpredict the number of bands and their relative intensities, which might be the result of neglecting triple combination bands (Maltseva et al. 2015). However, previous theoretical studies did not consider triple combination bands, due to the fact that 1–3 and 2–2 Darling–Dennison resonances could not be included in their program (Mackie et al. 2015, 2016, 2018).

Figure 7 shows a comparison between the high-resolution experimental spectrum of naphthalene and the calculated anharmonic spectra with different order-of-combination bands. As discussed in a recent article (Maltseva et al. 2015), four

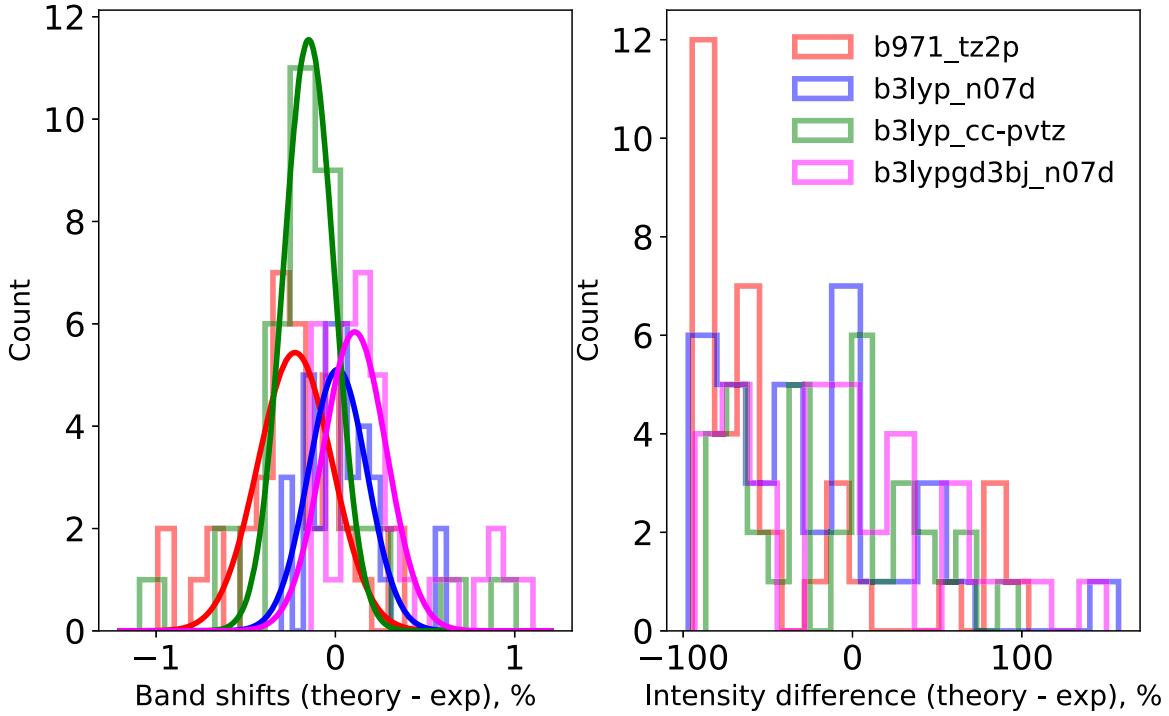

Figure 5. Histogram showing the differences between the line positions and intensities of the anharmonic theory (with different functionals and basis sets) and the high-resolution gas-phase experiments for naphthalene, anthracene, pyrene, and chrysene (Maltseva et al. 2016). Gaussian fittings are added for the histograms of band shifts.

Table 2
Parameters of Gaussian Profiles for the Histograms Associated with High-resolution Experimental Spectra; No Successful Gaussian Profile is Found for Relative Intensities

	Positions $Ae^{\frac{-(x-\mu)^2}{2\sigma^2}}$			Intensities $Ae^{\frac{-(x-\mu)^2}{2\sigma^2}}$		
Methods	A	μ	σ	A	μ	σ
B971/TZ2P	5.44	−0.23	0.21	...	...	...
B3LYP/N07D	5.11	0.01	0.16	...	...	...
B3LYP/cc-PVTZ	11.55	−0.15	0.14	...	...	...
B3LYP-D3/N07D	5.84	0.11	0.18	...	...	...

IR-active fundamentals are expected in the CH-stretching region of naphthalene at the harmonic level and combinatorial analysis predicts an additional 12 bands at the double combination band level (Maltseva et al. 2015). In contrast, the experiments identify 23 bands in this spectral region. Our calculations confirm that theory cannot reproduce the observed number of bands at the level of double combination bands. When triple combination bands are included, all 23 bands are found in our calculations. In addition, three more bands that could not be identified due to the limitations of experimental techniques (low signal-to-noise ratio) can now be predicted by the theory.

3.4. Temperature Effects

PAH molecules are excited by the absorption of a visible/UV photon and undergo internal conversion, where the excess energy is converted from electronic to nuclear degrees of freedom, while they relax to the electronic ground state. Subsequently, the energy is redistributed among the vibrational degree of freedom (intramolecular vibrational redistribution, IVR) and the vibrationally excited molecules cool down by emitting IR photons (Leger & Puget 1984). The corresponding spectra can be severely distorted and broaden due to the temperature effects (Chen et al. 2018). Therefore, for a comprehensive study of the spectral features of the interstellar PAHs, it is crucial to take the temperature effects into account.

We adopt the Wang-Landau method (Basire et al. 2009) for this purpose, in which the vibrational densities of states (DoSs) are calculated by a random walk in energy space. For each set of quantum numbers, the energy of the molecule can be calculated with the following formula:

$$E(n) = \sum_i h\nu_i\left(n_i + \frac{1}{2}\right) + \sum_{i\leqslant j}\chi_{ij}\left(n_i + \frac{1}{2}\right)\left(n_j + \frac{1}{2}\right), \quad (9)$$

where $n \equiv (n_1, n_2, \ldots)$, are the quantum numbers representing the states of each vibrational mode. The harmonic vibrational frequencies ν_i and anharmonic couplings χ_{ij} are extracted from above anharmonic IR calculations.

The temperature effects can be incorporated through a second Monte Carlo simulation in the space of quantum numbers. At each Monte Carlo step, line position shifts can be estimated by the following formula:

$$\Delta\nu^{(k)}(\{n\}) = \omega_k + 2\chi_{kk} + \frac{1}{2}\sum_{i\neq k}\chi_{ik} + 2\chi_{kk}n_k + \sum_{i\neq k}\chi_{ik}n_i, \quad (10)$$

where ω_k is the fundamental band.

The accumulated absorption $S(\nu, E)$ at wavelength ν and for a broad range of internal energies E is given by

$$S(\nu, E) = \sum_{\text{MCsteps}}\sum_k (n_k + 1)I_k\delta[\nu - \Delta\nu^{(k)}], \quad (11)$$

where I_k is the intensity of vibrational mode k.

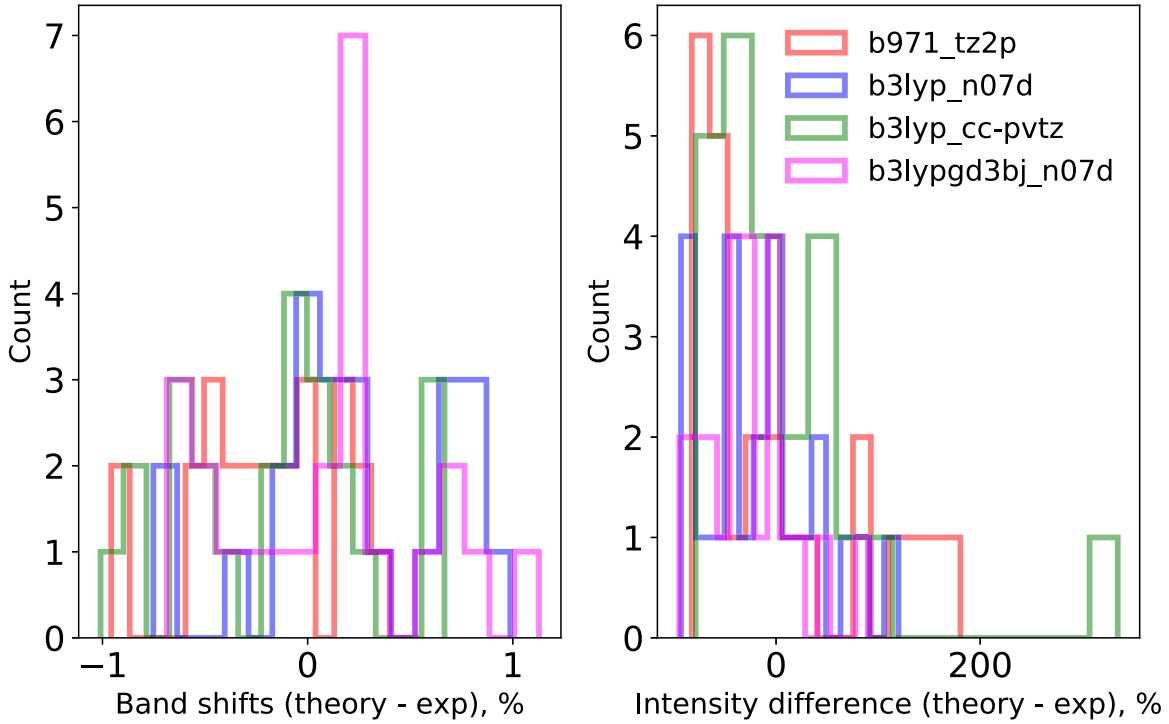

Figure 6. Histogram showing the differences between the line positions and intensities of the anharmonic theory (with different functionals and basis sets) and the high-resolution gas-phase experiments measured for 9,10-dimethylanthracene and 9,10-dihydroanthracene (Mackie et al. 2018). Due to poor statistics, no Gaussian fitting is achieved.

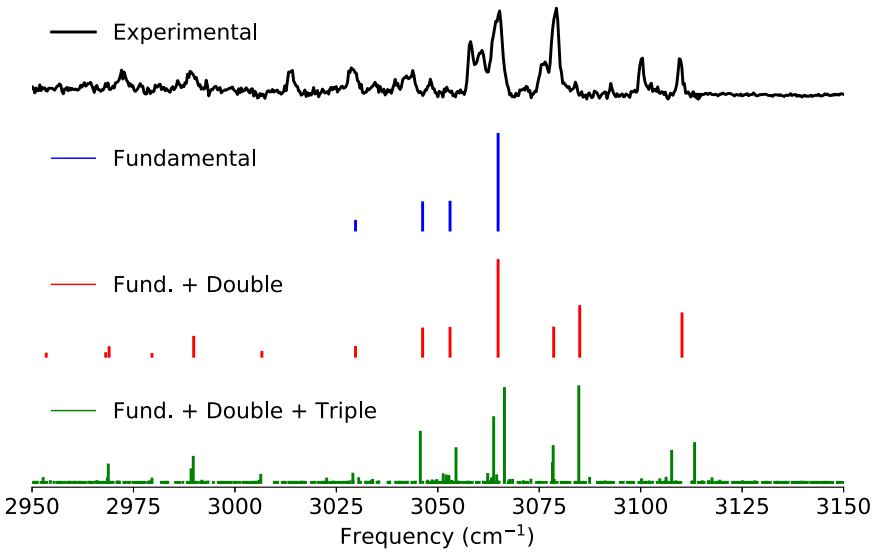

Figure 7. Comparison of high-resolution gas-phase experimental IR spectra and calculated spectra for naphthalene. The blue sticks represent fundamental bands. The red sticks are a combination of fundamental and double combination bands. The green sticks show the superposition of fundamental, double, and triple combination bands.

The temperature spectrum $S(\nu, T)$ can be derived by a standard Laplace transformation of $S(\nu, E)$:

$$S(\nu, T) = \frac{1}{Z}\int S(\nu, E)\Omega(E)e^{-E/k_BT}dE, \quad (12)$$

where $\Omega(E)$ is the DoS at energy E, and the partition function can be found by the following equation:

$$Z = \int \Omega(E)e^{-E/k_BT}dE. \quad (13)$$

Figure 8 shows a comparison between calculated anharmonic spectra at 0 and 1000 K. One can see that at 0 K, the spectrum is composed of discrete individual vibrational modes, including fundamental and combination bands. However, due to the temperature effects, the bands are shifted and broadened. A continuous spectrum with linked broad bands shows up as the temperature increases.

3.5. Comparison to the Observational IR Spectra

It is generally accepted that PAHs are responsible for the AIBs, in which the 3.3 μm band is attributed to the C–H stretching modes of neutral PAHs. Meanwhile the other bands, i.e., 6.2 μm, 7.7 μm, 8.6 μm, 11.2, and 12.7 might have

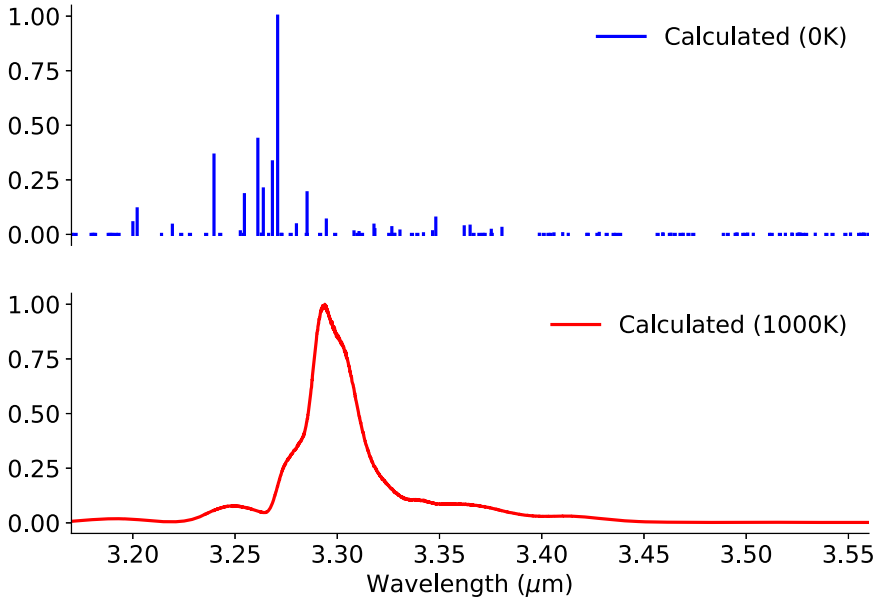

Figure 8. The temperature effects on anharmonic spectra of pyrene. The blue sticks show the position of various fundamental and combination bands at 0 K. The red curve represents the IR spectra at 1000 K.

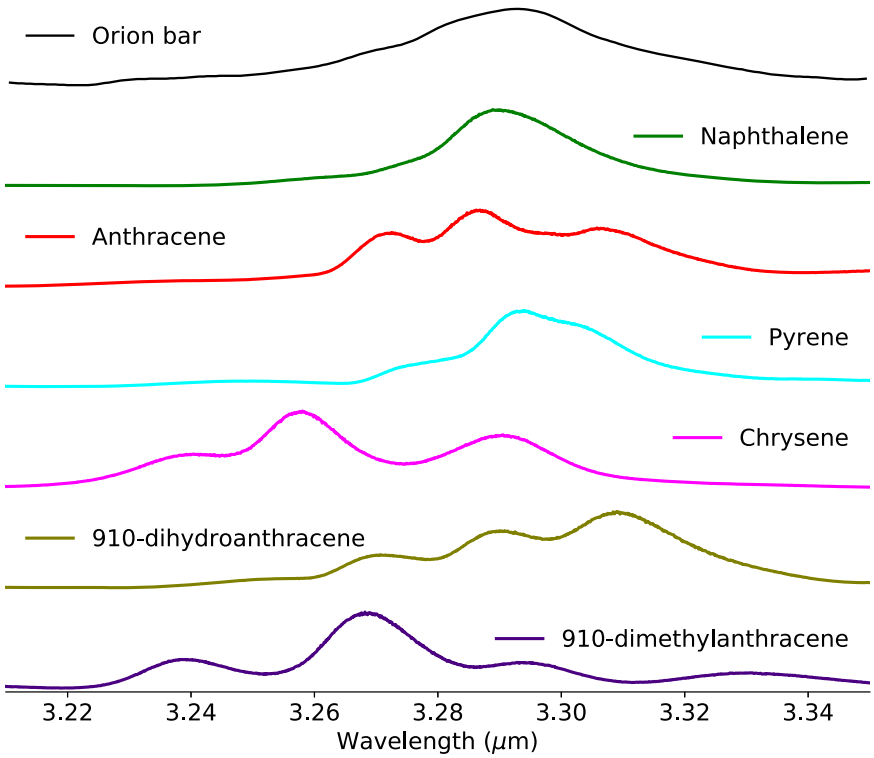

Figure 9. Comparison of the observational IR spectra of Orion bar and calculated spectra of several PAHs at 1000 K. The observational data are retrieved from the *Infrared Space Observatory* archive.

different origins, e.g., mixed large PAHs (Bauschlicher et al. 2008), charged PAHs (Bauschlicher et al. 2009), or nitrogen-substituted PAHs (Hudgins et al. 2005), etc. This work focuses on the neutral system. Figure 9 shows the C–H stretching of the calculated anharmonic IR spectra of six PAHs at 1000 K in comparison to the observational spectrum of the Orion bar observed by the *Infrared Space Observatory*. The spectra of naphthalene and pyrene seem to agree the best with the observational spectra, in regard to band positions and band profiles. The rest of the molecules show additional features that cannot be identified clearly in the observational spectrum. Large compact PAHs, e.g., circumcoronene ($C_{54}H_{18}$), circumovalene ($C_{66}H_{20}$), etc., were expected to be the carrier of the AIBs (Bauschlicher et al. 2008). However, due to the limitations of the time-independent methods, the anharmonic IR spectra of such large and highly symmetric species cannot be produced. To study the anharmonic and high-temperature features of large PAHs, new and innovative methods are

required, e.g., molecular dynamics simulations. See our follow-up articles for details on such studies.

4. Conclusions

In this work, we study four different combinations of functional and basis sets to compute the anharmonic spectrum of six PAHs. The low-resolution gas-phase experimental spectra downloaded from the NIST Chemistry WebBook website (Linstrom & Mallard 2001) and high-resolution low-temperature gas-phase experimental spectra reported recently (Maltseva et al. 2015, 2016; Mackie et al. 2018) are used as references. Quantitative comparisons are performed to identify the best functional and basis sets in agreement with the experimental spectra. The resonant thresholds influence the anharmonic IR spectra systematically: when the thresholds increase, the whole spectrum shifts to higher wavenumbers. The threshold value of 200 cm^{-1} presents reasonable band positions and relative intensities, and it takes reasonable computational time and memory. Higher thresholds incorporate more interactions, and thus require more extensive consumption of computational time and memory.

Compared with the NIST data, B3LYP/N07D shows the highest and thinnest Gaussian profile for describing the band positions. B971/TZ2P comes next. In regard to Gaussian height, B3LYP-D3/N07D comes third. The worst one is B3LYP/cc-PVTZ. Regarding the intensities, B3LYP/cc-PVTZ shows the best agreement with the intensities of experimental spectra. The second best method is B3LYP/N07D. Then come B3LYP-D3/N07D and B971/TZ2P.

Compared with the high-resolution experimental data, B3LYP/cc-PVTZ is superior in terms of band positions to any other tested methods. For the relative intensities, due to the shortage of data points and wide distribution of the histogram, no successful Gaussian fitting is found. However, it is clear that B971/TZ2P shows the highest bar on the histogram.

For decorated PAHs, due to the poor statistics, no successful Gaussian fitting is achieved. Judging by the distribution of the data, B3LYP-D3/N07D is the most accurate method for describing the band positions, and B3LYP/cc-PVTZ is the most accurate method for describing the relative intensities.

Higher-order combination bands are found to be crucial for understanding the delicate structures of the spectrum, especially for the C–H stretching region: bands that could not be described at the level of double combination bands can now be adequately explained by triple combination bands.

In addition the anharmonicity and resonances, temperature effects play a vital role in interpreting the observational IR spectra. The Wand-Landau random walk technique (Wang & Landau 2001) is applied to the calculated anharmonic IR spectra. Combining the Wand-Landau technique with GVPT2 calculations, we compute the anharmonic spectra at a fixed temperature. It has been shown that the fixed high-temperature spectra are in good agreement with the measured emission spectra in peak position, overall band profile, and bandwidth (Joblin et al. 1994; Cook et al. 1996). The comparisons between observational and calculated high-temperature spectra indicate that the carrier of AIB at 3.3 μm might be small and compact PAHs, such as naphthalene and pyrene. Larger PAHs or decorated PAHs bring additional bands that cannot be identified in the observational spectra.

This work is supported by the Swedish Research Council (Contract No. 2015-06501). The facility is supported by the Swedish National Infrastructure for Computing (Project No. SNIC 2018/3-30). The calculations were carried out on Kebnekaise and Abisko located at the High Performance Computing Center North (HPC2N).

ORCID iDs

Tao Chen https://orcid.org/0000-0003-4145-4300

References

Allamandola, L., Tielens, A., & Barker, J. 1989, ApJS, 71, 733
Allen, W. D., Yamaguchi, Y., Császár, A. G., et al. 1990, CP, 145, 427
Amos, R. D., Handy, N. C., Green, W. H., et al. 1991, JChPh, 95, 8323
Assfeld, X., Almlöf, J. E., & Truhlar, D. G. 1995, CPL, 241, 438
Barone, V. 2004, JChPh, 120, 3059
Barone, V. 2005, JChPh, 122, 014108
Barone, V., Biczysko, M., & Bloino, J. 2014, PCCP, 16, 1759
Barone, V., Bloino, J., Guido, C. A., & Lipparini, F. 2010, CPL, 496, 157
Barone, V., & Cimino, P. 2008, CPL, 454, 139
Basire, M., Parneix, P., Calvo, F., Pino, T., & Bréchignac, P. 2009, JPCA, 113, 6947
Bauschlicher, C. W., Jr, Peeters, E., & Allamandola, L. J. 2008, ApJ, 678, 316
Bauschlicher, C. W., Jr, Peeters, E., & Allamandola, L. J. 2009, ApJ, 697, 311
Becke, A. D. 1992, JChPh, 96, 2155
Bloino, J., & Barone, V. 2012, JChPh, 136, 124108
Bloino, J., Biczysko, M., & Barone, V. 2012, Journal of Chemical Theory and Computation, 8, 1015
Boersma, C., Bregman, J., & Allamandola, L. 2013, ApJ, 769, 117
Boese, A. D., & Martin, J. M. 2004, JPCA, 108, 3085
Bowman, J. M. 1978, JChPh, 68, 608
Chen, T., Mackie, C., Lee, T. J., & Tielens, A. G. G. M. 2018, A&A, in press
Christoffel, K. M., & Bowman, J. M. 1982, CPL, 85, 220
Clabo, D. A., Allen, W. D., Remington, R. B., Yamaguchi, Y., & Schaefer, H. F. 1988, CP, 123, 187
Cook, D., Schlemmer, S., Balucani, N., et al. 1996, Natur, 380, 227
Csaszar, A. G. 2012, Wiley Interdisciplinary Reviews: Computational Molecular Science, 2, 273
Dunning, T. H., Jr 1971, JChPh, 55, 716
Dunning, T. H., Jr 1989, JChPh, 90, 1007
Frisch, M., Trucks, G., Schlegel, H., et al. 2016, Gaussian 16 (Wallingford, CT: Gaussian, Inc.)
Gaw, J. F., Willets, A., Green, W. H., & Handy, N. C. 1996, SPECTRO, version 3.0
Grimme, S., Ehrlich, S., & Goerigk, L. 2011, JCoCh, 32, 1456
Gruet, S., Pirali, O., Goubet, M., Tokaryk, D., & Brechignac, P. 2015, JPCA, 120, 95
Hamprecht, F. A., Cohen, A. J., Tozer, D. J., & Handy, N. C. 1998, JChPh, 109, 6264
Hudgins, D. M., Bauschlicher, C. W., Jr, & Allamandola, L. 2005, ApJ, 632, 316
Joblin, C., d'Hendecourt, L., Léger, A., & Defourneau, D. 1994, A&A, 281, 923
Jung, J. O., & Gerber, R. B. 1996, JChPh, 105, 10332
Krasnoshchekov, S. V., Isayeva, E. V., & Stepanov, N. F. 2014, JChPh, 141, 234114
Kubatkin, S., Danilov, A., Hjort, M., et al. 2003, Natur, 425, 698
Langhoff, S. R. 1996, JPhCh, 100, 2819
Lee, C., Yang, W., & Parr, R. G. 1988, PhRvB, 37, 785
Lee, T. J., Martin, J. M., & Taylor, P. R. 1995, JChPh, 102, 254
Leger, A., & Puget, J. 1984, A&A, 137, L5
Li, A. 2009, Deep Impact as a World Observatory Event: Synergies in Space, Time, and Wavelength (Berlin: Springer), 161
Linstrom, P. J., & Mallard, W. G. 2001, Journal of Chemical & Engineering Data, 46, 1059
Mackie, C. J., Candian, A., Huang, X., et al. 2015, JChPh, 143, 224314
Mackie, C. J., Candian, A., Huang, X., et al. 2016, JChPh, 145, 084313
Mackie, C. J., Candian, A., Huang, X., et al. 2018, PCCP, 20, 1189
Maltseva, E., Mackie, C. J., Candian, A., et al. 2018, arXiv:1802.01497
Maltseva, E., Petrignani, A., Candian, A., et al. 2015, ApJ, 814, 23
Maltseva, E., Petrignani, A., Candian, A., et al. 2016, ApJ, 831, 58
Martin, J. M., Lee, T. J., & Taylor, P. R. 1998, JChPh, 108, 676

Martin, J. M., Lee, T. J., Taylor, P. R., & François, J.-P. 1995, JChPh, 103, 2589
Maslen, P. E., Handy, N. C., Amos, R. D., & Jayatilaka, D. 1992, JChPh, 97, 4233
Ravichandran, L., & Banik, S. 2018, Theoretical Chemistry Accounts, 137, 1
Ricca, A., Bauschlicher, C. W., Jr, Boersma, C., Tielens, A. G., & Allamandola, L. J. 2012, ApJ, 754, 75
Richter, H., & Howard, J. B. 2000, PrECS, 26, 565
Rosnik, A. M., & Polik, W. F. 2014, MolPh, 112, 261
Srogi, K. 2007, Environmental Chemistry Letters, 5, 169
Tielens, A. G. G. M. 2008, ARA&A, 46, 289
Tielens, A. G. G. M. 2013, RvMP, 85, 1021
Wang, F., & Landau, D. 2001, PhRvL, 86, 2050
Wang, X., Zhi, L., Tsao, N., et al. 2008, Angewandte Chemie International Edition, 47, 2990
Yagi, K., Taketsugu, T., Hirao, K., & Gordon, M. S. 2000, JChPh, 113, 1005